Structural and physical properties of $SrMn_{1-x}Ru_xO_3$ perovskites

S. Kolesnik, B. Dabrowski, and O. Chmaissem
Department of Physics, Northern Illinois University, DeKalb, Illinois 60115, USA
and Materials Science Division, Argonne National Laboratory, Argonne, Illinois 60439, USA
(Received 28 February 2008; revised manuscript received 17 July 2008; published 18 December 2008)

We combine the results of magnetic and transport measurements with neutron-diffraction data to construct the structural and magnetic phase diagram of the entire family of $SrMn_{1-x}Ru_xO_3$ ($0 \le x \le 1$) perovskites. We have found antiferromagnetic (AF) ordering of the *C* type for lightly Ru-substituted materials ($0.06 \le x \le 0.5$) in a similar manner to $R_ySr_{1-y}MnO_3$ (R=La,Pr) due to the generation of Mn^{3+} in both families of manganite perovskites by either *B*-site substitution of Ru^{5+} for Mn^{4+} or *A*-site substitution of R^{3+} for Sr^{2+}. This similarity is driven by the same ratio of d^4/d^3 ions in both classes of materials for equivalent substitution level. In both cases, a tetragonal lattice distortion is observed, which for some compositions ($0.06 \le x \le 0.2$) is coupled to a *C*-type AF transition and results in a first-order magnetic and resistive transition. Heavily substituted $SrMn_{1-x}Ru_xO_3$ materials are ferromagnetic due to dominating exchange interactions between the Ru^{4+} ions. Intermediate substitution ($0.6 \le x \le 0.7$) leads to a spin-glass behavior instead of a quantum critical point reported previously in single crystals due to enhanced disorder.

DOI: 10.1103/PhysRevB.78.214425 PACS number(s): 75.30.Kz, 75.50.Ee, 75.50.Lk, 81.30.Dz

I. INTRODUCTION

The substitution of Ru in perovskite manganites has been demonstrated to lead to a variety of interesting physical phenomena. For colossal magnetoresistance manganites $La_{0.5}Sr_{0.5}Mn_{1-y}Ru_yO_3$ with ferromagnetic (FM) matrix and $La_{0.45}Sr_{0.55}Mn_{1-y}Ru_yO_3$ with antiferromagnetic (AF) matrix, the low Ru doping $0.05 \le y \le 0.15$ induces an enhanced ferromagnetism with an increasing Curie temperature T_C.[1] Ru ions in these materials exist mainly in the form of Ru^{4+} with a small quantity of Ru^{5+}. A ferromagnetic exchange interaction between Mn^{3+} and $Ru^{4+}(Ru^{5+})$ has been attributed to this enhancement of ferromagnetism.[1] Similarly in charge-ordered $Nd_{0.5}Sr_{0.5}MnO_3$, T_C is significantly increased by substitution of Ru^{4+} but the charge ordering can be destroyed.[2] The incorporation of Ru ions in $CaMn_{1-y}Ru_yO_3$ perovskites can induce ferromagnetism in a large substitution range $0.1 \le y \le 0.8$ with a maximum Curie temperature of $T_C = 210$ K for $y=0.4$ and a metallic character for $0.2 \le y \le 0.4$.[3] By substitution of only a few percent of Ru with Mn in $Sr_3(Ru_{1-y}Mn_y)_2O_7$, the ground state can be switched from a paramagnetic metal to an antiferromagnetic insulator.[4]

The study of $SrRu_{1-y}Mn_yO_3$ single crystals in the limited (Ru-rich) range of compositions $0 \le y \le 0.6$ has shown that the Mn substitution can drive the system from the itinerant FM state for $SrRuO_3$ through a "quantum critical point" at $y_c=0.39$ to an insulating AF state.[5] Sahu *et al.*[6,7] reported a contradictory finding that the ferromagnetic state may still be observed with higher Mn contents including $SrRu_{0.5}Mn_{0.5}O_3$ for polycrystalline samples prepared in air at 1200 °C. A more complicated phase diagram with the coexistence of FM and AF phases in a wide range of substitution and a large magnetoresistance have been reported by Zhang *et al.*[8] for polycrystalline samples prepared in air at 1150 °C. The discrepancy can be traced to the highly inhomogeneous polycrystalline samples obtained to date, containing a large amount of $SrRuO_3$, for which only a fraction of the FM phase changes but not the magnetic phase or transition temperature (see Fig. 1 of Ref. 6, Fig. 2 of Ref. 7, Fig. 3 of Ref. 8, and Fig. 3 of Ref. 9).

One end member of the $SrMn_{1-x}Ru_xO_3$ family, $SrRuO_3$, is a unique ferromagnetic metal among 4*d* transition-metal-based perovskite oxides. Most dopants for low-spin Ru^{4+} (t_{2g}^4) decrease the ferromagnetic Curie temperature from 163 K, except for Cr.[10–12] The other end member, a cubic perovskite $SrMnO_3$ is a *G*-type antiferromagnet with $T_N=233$ K. The oxidation state of Mn in the latter material is also 4+. If this valency of Mn is preserved (e.g., as in $Sr_{1-y}Ca_yMnO_3$), then the *G*-type AF ordering is observed in the cubic, tetragonal, and orthorhombic crystal structures.[13] T_N is suppressed by the deviation of the Mn-O-Mn bond angle from 180° and by the variance of the average size of the *A*-site ion via changes in the Sr/Ca ratio.[13,14]

The substitution of Ru^{5+} for Mn^{4+} in $SrMnO_3$ was considered[15] to stabilize the cubic perovskite structure by the induced Mn valency shift, corresponding to electron doping by Mn^{3+} in the Mn^{4+} matrix. The $L_{2,3}$-edge absorption spectroscopy of Ru and Mn in Ru-rich $SrRu_{1-y}Mn_yO_3$ ($0 \le y \le 0.5$) has revealed the mixed valence of both Mn^{3+}/Mn^{4+} and Ru^{4+}/Ru^{5+}.[7] ^{55}Mn NMR on $SrRu_{0.9}Mn_{0.1}O_3$ has demonstrated that Mn exists in an intermediate $Mn^{3+/4+}$ valence state due to fast electron hopping.[16]

In this study, we investigate the complete solubility range of polycrystalline $SrMn_{1-x}Ru_xO_3$ samples and construct the phase diagram of structural, magnetic, and conducting properties. The polycrystalline samples were characterized by neutron-diffraction, magnetic, transport, and thermoelectric experiments. The incorporation of Ru in the $SrMnO_3$ matrix ($0.06 \le x \le 0.2$) results in a phase transition to a *C*-type antiferromagnetic state accompanied by a cubic-tetragonal transition. At slightly higher substitutions ($0.3 \le x \le 0.5$) the structural transition temperature is higher than the AF transition temperature. The intermediate substitution level ($0.6 \le x \le 0.7$) induces a spin-glass behavior due to competing ferromagnetic and antiferromagnetic interactions in the tetragonal structure. Close to the maximum Ru substitution

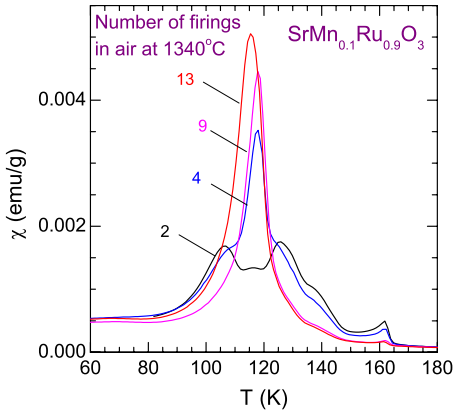

FIG. 1. (Color online) Magnetic ac susceptibility for the $SrMn_{0.1}Ru_{0.9}O_3$ sample after increasing number of firings. A magnetically single-phase material is obtained after 13 grindings and firings.

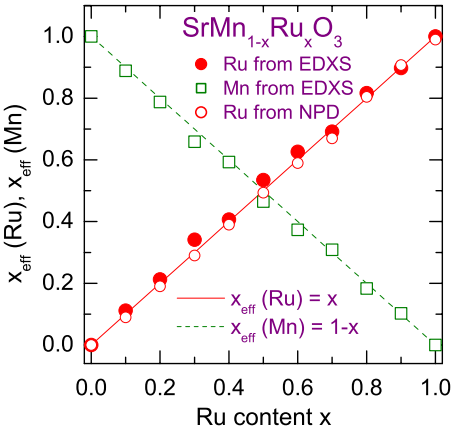

FIG. 2. (Color online) The effective contents of Ru and Mn ions for $SrMn_{1-x}Ru_xO_3$ from the EDXS. The straight lines are the nominal contents of both cations. The statistical errors are within the marker symbols. The refined Ru contents from NPD are shown as open circles.

$(0.8 \leq x \leq 1)$ the material becomes ferromagnetic in the orthorhombic structure.

II. EXPERIMENTAL DETAILS

Samples with $x \leq 0.5$ were prepared using a two-step synthesis method developed for similar kinetically stable perovskites.[17] First, oxygen-deficient samples were prepared in argon at $T=1300-1400$ °C. The samples were then annealed in air at lower temperatures to achieve stoichiometric compositions with respect to the oxygen content. The samples with $x>0.5$ were prepared in air at 1330–1340 °C with many (up to 14) intermittent grindings due to difficulty of achieving homogeneous material. An excess of RuO_2 was added to compensate for Ru loss due to sublimation at these high temperatures. The process of formation of single-phase and homogeneous materials was monitored with x-ray diffraction (Rigaku D/MAX diffractometer) and ac susceptibility (physical property measurement system model 6000) (Quantum Design) measurements. After a few firings, x-ray diffraction indicated formation of single-phase material, though the ac susceptibility measurements clearly showed peaks related to multiple magnetic transitions and hence highly inhomogeneous samples. Figure 1 shows a sequence of ac susceptibility measurements for the $SrMn_{0.1}Ru_{0.9}O_3$ sample, which demonstrates the gradual improvement of sample quality. This difficulty to achieve research quality polycrystalline materials may explain the discrepancy in the properties of single crystals and bulk samples reported to date.

The ac susceptibility, resistivity, thermal conductivity, and Seebeck coefficient were measured using a physical property measurement system model 6000 (Quantum Design). The dc magnetization was measured using a magnetic property measurement system model MPMS-7 (Quantum Design). Time-of-flight neutron powder-diffraction (NPD) data were collected at 300 K (room temperature) for all members of the $SrMn_{1-x}Ru_xO_3$ series on the special environment powder diffractometer (SEPD) (Ref. 18) at the intense pulsed neutron source (IPNS) at Argonne National Laboratory. Data were collected, for the $x=0.2$, 0.7, and 0.9 samples, at several temperatures between 10 and 320 K using a closed cycle refrigerator. In the refinements, high-resolution backscattering data, from 0.5 to 4 Å d spacing, were analyzed using the Rietveld method and the general structure analysis system (GSAS) code.[19] Absorption, background, and peak width parameters were refined, together with the lattice parameters, atomic positions, and isotropic and anisotropic temperature factors for the cations and oxygen atoms, respectively.

The cationic ratio was determined by energy dispersive x-ray spectroscopy (EDXS) analysis in a Hitachi S-4700-II scanning electron microscope at the Electron Microscopy Center, Argonne National Laboratory. Typically, five spot spectra were collected across the surface of sintered pellets. Figure 2 presents the effective contents x_{eff} of Ru and Mn ions calculated from the EDXS spectra using a normalization condition $x_{\text{eff}}(\text{Ru})+x_{\text{eff}}(\text{Mn})=1$. We observe a good agreement with the nominal compositions drawn as straight lines in Fig. 2. This result is strongly supported by the refined Ru occupancies from the neutron powder-diffraction data.

III. RESULTS AND DISCUSSION

A. Neutron powder diffraction and structural details

The well-known perovskite structures of the two end members of the series, namely, $SrMnO_3$ and $SrRuO_3$, have frequently been described as crystallizing in the cubic and orthorhombic space-group symmetries, respectively. The Ru spins, in $SrRuO_3$, do not localize (are itinerant) and the material is viewed as an itinerant ferromagnet below 163 K. On the other hand, in $SrMnO_3$, the Mn spins become localized below 233 K in a G-type antiferromagnetic structure.

Room-temperature structural refinements ($T=300$ K) for all members of the $SrMn_{1-x}Ru_xO_3$ series demonstrate that upon increasing x, the symmetry changes from cubic $Pm\bar{3}m$ $(x \leq 0.2)$ to tetragonal $I4/mcm$ (for $0.3 \leq x \leq 0.7$) to orthorhombic $Pbnm$ for $(x \geq 0.8)$, which is in a good agreement with the different magnetic and resistive properties of the

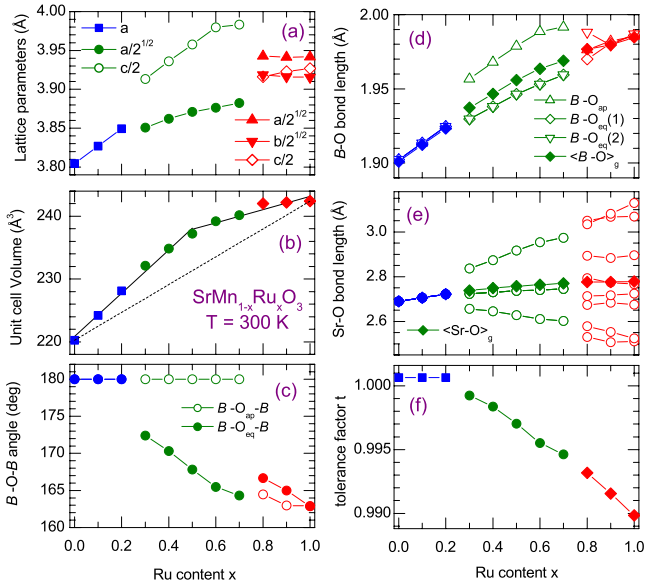

FIG. 3. (Color online) Room-temperature structural parameters refined from neutron diffraction for $SrMn_{1-x}Ru_xO_3$. *B* is the *B*-site ion Ru or Mn. [(a), (b), and (f)] Squares denote a cubic $Pm\bar{3}m$ structure, circles denote a tetragonal $I4/mcm$, and diamonds denote an orthorhombic *Pbnm*. [(d) and (e)] Open symbols: individual bond lengths; full symbols: geometrical average. (f) The tolerance factor is defined as $\langle \text{Sr-O} \rangle / (\langle B\text{-O} \rangle \sqrt{2})$. The dashed line in (b) represents Vegard's law; the solid lines in (b) are linear fits to the data (see text).

materials discussed in Secs. III B–III D. Refined Ru and Mn site occupancies were in agreement with the nominal values, within one to three standard deviations, as shown in Fig. 2. Refined structural parameters are presented in Fig. 3 as a function of composition. The lattice parameters [Fig. 3(a)] display overall increase associated with a larger ionic size of Ru^{4+} (the average bond length of $\langle Ru^{4+}\text{-O} \rangle = 1.985$ Å) than Mn^{4+} (the average bond length of $\langle Mn^{4+}\text{-O} \rangle = 1.903$ Å), as observed in Fig. 3(d). The sequence of structural transitions from high-symmetry cubic $Pm\bar{3}m$ to low-symmetry orthorhombic *Pbnm* is thus a consequence of decreasing tolerance factor of the perovskite structure $t(x) = \langle \text{Sr-O} \rangle / \sqrt{2} \langle B\text{-O} \rangle$ (*B* =Mn,Ru) from 1 to 0.99 [Fig. 3(f)]. Similar sequence of transitions was observed for $Sr_{1-x}Ca_xMnO_3$, for which decrease in tolerance factor was a result of smaller ionic size of Ca than Sr.[13] Since neutron diffraction found no evidence for Mn/Ru cation ordering at any *x*, the volume would be expected to vary linearly with *x* according to the Vegard law presented as a dashed line in Fig. 3(b). However, the unit-cell volume exhibits deviations from the linear behavior especially when crossing from the Mn-rich side to the Ru-rich side of the phase diagram [Fig. 3(b)]. These deviations can be solely explained by geometrical considerations of the charge transfer $Ru^{4+}(0.62\ \text{Å}) + Mn^{4+}(0.53\ \text{Å}) \rightarrow Ru^{5+}(0.565\ \text{Å}) + Mn^{3+}(0.645\ \text{Å})$ from the fact that the average ionic size of a Ru^{5+}, Mn^{3+} pair (0.605 Å) is larger than that of a Ru^{4+}, Mn^{4+} pair (0.575 Å). Following the procedure developed by Williams *et al.*[12] for $SrRu_{1-y}Cr_yO_3$, we made linear fits to the data in Fig. 3(b) and obtained a good agreement of the charge-transfer model with the data. A similar phenomenon has recently been observed[20] in $CaRu_{1-y}Mn_yO_3$ and also interpreted in terms of mixed valence Ru^{4+}, Ru^{5+}, Mn^{4+}, and Mn^{3+} ions. The latter compound preserves its orthorhombic *Pnma* structure within the entire composition range.

Another anomalous feature observed in the data is a large increase in the average ⟨Sr-O⟩ bond length from 2.69 to 2.78 Å [Fig. 3(e)]. In order to interpret the "abnormal" behavior of the ⟨Sr-O⟩ bond length, we performed simple bond valence sum calculations[21] from which we find the calculated oxidation state $v(\text{Sr})$ of Sr to decrease from 2.5 to 2.0 as the Ru content increases from 0 to 1. The unphysical values of the Sr oxidation state [i.e., when $v(\text{Sr}) > 2$] may be interpreted as evidence for the presence of significant strains in the Mn-rich side of the phase diagram with the strains relaxing as a function of increased Ru content. Strain relaxation would then occur through a series of structural distortions from heavily stressed cubic to moderately stressed tetragonal and finally to "stress-free" orthorhombic structures. Further evidence for stress relaxation may be observed in the behavior of the unit-cell volume as seen in the change in slope in Fig. 3(b). Additionally, a changeable ⟨Sr-O⟩ bond length could also be due to the decreasing size of the oxygen ion as a function of hole transfer to it from Mn, i.e., formation of the ligand holes for $SrMnO_3$ compound. The Mn to O charge transfer would not lead to a large change in the ⟨Mn-O⟩ bond length as the overall amount of charge remains constant on the electronically relevant Mn-O network. Another possibility would be that the ⟨Sr-O⟩ bond lengths are simply changeable depending on the *B*-site ion of the perovskite structure. To unambiguously differentiate between these possibilities extensive x-ray absorption spectroscopy studies would be necessary for both transition metal and oxygen ions. We point out here, however, that peculiar magnetic properties of $SrMnO_3$ and lightly substituted compounds, which are discussed in Sec. III B, may be caused by the charge transfer from Mn to O ions.

Evolution of the structure of the $x = 0.2$ sample as a function of temperature is shown in Fig. 4. At temperatures above 260 K, the paramagnetic material is best described using the cubic $Pm\bar{3}m$ symmetry. Below 260 K, a structural phase transition takes place to lower tetragonal $I4/mcm$ space-group symmetry and additional antiferromagnetic peaks become visible. In this space group, a good fit to the magnetic intensities could only be achieved by further lowering the magnetic symmetry to $I_p4/mc'm'$. In this magnetic symmetry, long-range ordering of *c* axis oriented Ru/Mn spins takes place to form *C*-type antiferromagnetically coupled FM chains.

Temperature-dependent neutron-diffraction patterns for the tetragonal $x = 0.7$ and orthorhombic $x = 0.9$ samples show no structural change and no extra magnetic intensities at any temperature between 10 and 300 K that are in good agreement with the material spin-glass and itinerant ferromagnetic properties, respectively. A decrease in the difference between individual *B*-O bonds [Fig. 4(e)] with increasing temperature as well as a similar effect for lattice parameters [Fig. 4(f)] and *B*-O-*B* bond angles [Fig. 4(h)] indicate an incipient transition to the cubic phase for the $x = 0.7$ composition. No such behavior is observed for the orthorhombic $x = 0.9$ composi-

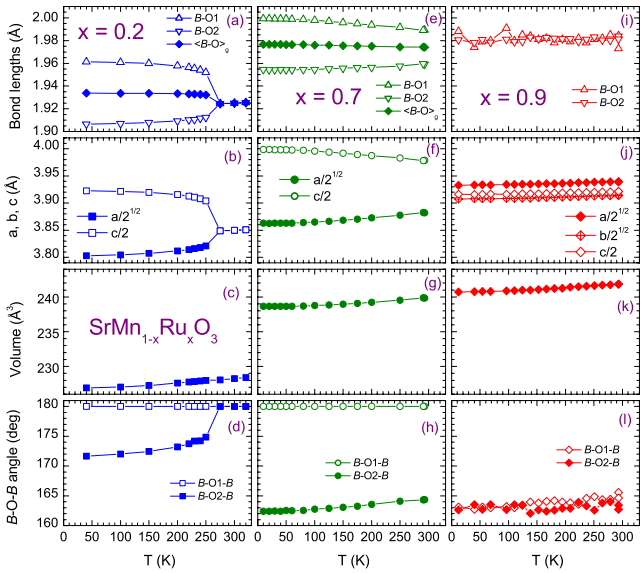

FIG. 4. (Color online) Temperature dependence of the refined structural parameters for three $SrMn_{1-x}Ru_xO_3$ samples: [(a)–(d)] $x=0.2$, [(e)–(h)] $x=0.7$, and [(i)–(l)] $x=0.9$. B is the B-site ion Ru or Mn. [(a) and (e)] Open symbols: individual bond lengths; full symbols: geometrical average.

tion, for which structural transitions to tetragonal and cubic phases appear to remain at high temperatures similar to $SrRuO_3$.[22] In addition, the $x=0.9$ composition does not exhibit a distinctive invar effect, which was observed below Curie temperature for $SrRuO_3$.[23] Suppression of the invar effect with a small amount of Mn substitution in $SrRuO_3$ is similar to both Cr and La substitution,[24,25] and introduction of Ru vacancy.[26]

B. Magnetic properties

The dc magnetization measured on cooling in a magnetic field of 1 kOe is presented in Fig. 5. From these results we

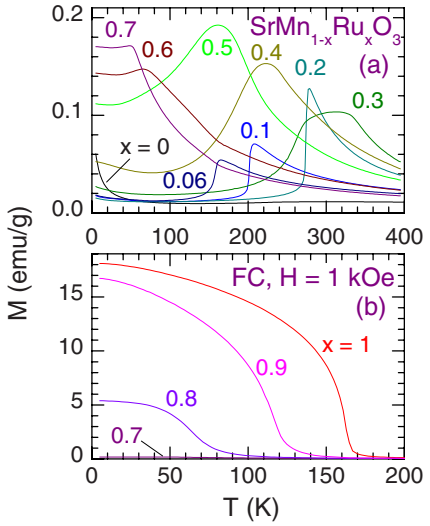

FIG. 5. (Color online) dc magnetization for $SrMn_{1-x}Ru_xO_3$ samples.

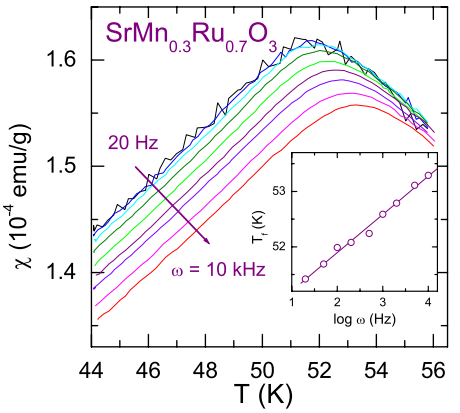

FIG. 6. (Color online) Temperature dependence of ac susceptibility for $SrMn_{0.3}Ru_{0.7}O_3$ at several frequencies. Inset shows the linear dependence of T_f on logarithmic frequency.

have determined Néel and Curie temperatures T_N and T_C (defined as the temperatures for which the slope of magnetization dM/dT is maximum and minimum, respectively). On the substitution of small amount of Ru for Mn ($0.06 \leq x \leq 0.2$), we observe sharp magnetic transitions from paramagnetic to a C-type AF ordered state. The Néel transitions in this substitution range are coupled with the structural cubic-tetragonal transitions, i.e., $T_N=T_s$. This type of behavior has also been observed for Sr-rich $R_ySr_{1-y}MnO_3$ (R=La, Pr).[27] For larger x, the structural transition takes place at temperatures T_s higher than T_N. As a result, the magnetic transition is not as sharp and an anomalous magnetization is observed for $x=0.3$ in $T_N \leq T \leq T_s$ before the material becomes paramagnetic above T_s. Further Ru doping decreases T_N, which is maximum for $x \sim 0.2-0.3$. More substitution of Ru leads to a change in the magnetic ordering from AF to FM, although this boundary is not as sharp as reported for single crystals,[5] but it is spread over a range of compositions ($0.6 \leq x \leq 0.7$) where a spin-glass behavior can be observed. In this range of substitution we also observed a cusp in the ac susceptibility, which supports the spin-glass behavior.

In Fig. 6, we present the ac susceptibility for $SrMn_{0.3}Ru_{0.7}O_3$ measured at several frequencies ω in an ac magnetic field of 14 Oe. One can observe a cusp in the ac susceptibility related to spin-glass behavior, a decrease in the ac susceptibility below T_f with increasing frequency, and a shift of T_f toward higher temperatures. The linear fit to $T_f(\log \omega)$ gives relative temperature shift vs frequency $\Delta T_f/[T_f \Delta(\log \omega)]=0.0136 \pm 0.005$. This value is similar to those observed for the $SrMn_{1-x}Fe_xO_3$ perovskite having mixed FM and AF interactions.[28] The spin-glass-related irreversibility between the "zero-field-cooled" and "field-cooled" magnetizations can also be observed (not shown). For lower Ru contents, ($0.4 \leq x \leq 0.6$) this kind of irreversibility, resembling a spin-glass behavior, can also be observed at temperatures below ~60 K in the AF state. This points to a frustrated or disordered AF state,[28] which is sometimes confused with spin-glass behavior.[8] A closer inspection of the remanent magnetization after "field cooling" shows that a slight irreversibility persists up to T_N in these compositions, which points to a certain level of disorder in the AF state.

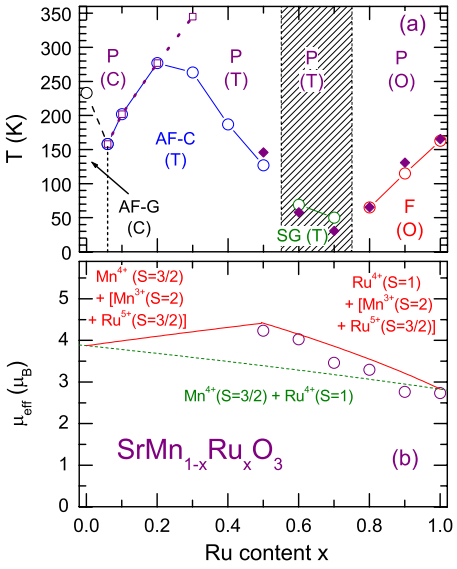

FIG. 7. (Color online) (a) Phase diagram for $SrMn_{1-x}Ru_xO_3$. Labels denote magnetic states [P, AF-G, AF-C, SG, and FM are paramagnetic, antiferromagnetic (type *G*), antiferromagnetic (type *C*), spin glass, and ferromagnetic, respectively]. Labels in parentheses denote crystal symmetry (C, T, and O are cubic, tetragonal, and orthorhombic, respectively). Open circles are magnetic transitions. Open squares are structural cubic to tetragonal transitions. Full diamonds are paramagnetic Curie-Weiss temperatures. The hatched area is an approximate boundary of magnetically frustrated region between the AF-C and FM states. (b) The effective paramagnetic moment μ_{eff} for $SrMn_{1-x}Ru_xO_3$. The lines denote various models describing possible oxidation states of Ru and Mn ions (see text)

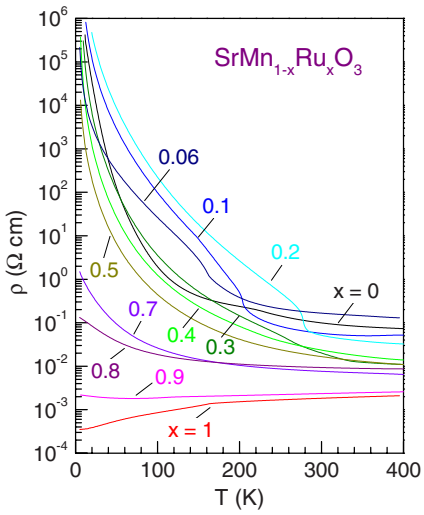

FIG. 8. (Color online) Temperature dependence of resistivity for $SrMn_{1-x}Ru_xO_3$ samples.

The phase diagram in the low Ru substitution regime presented in Fig. 7(a) strikingly resembles the phase diagram for $R_ySr_{1-y}MnO_3$ (R=La,Pr).[27] In both classes of materials, the two different substitutions in the parent $SrMnO_3$ compound, *A*-site substitution and *B*-site substitution, respectively, change the band filling by generating exactly the same amount of Mn^{3+} ions for the same substitution level. The concentration of these ions is not sufficient to induce Mn^{3+}-Mn^{4+} double exchange interaction but can induce the same tetragonal lattice distortion coupled with a *C*-type AF transition. The only magnetic ions present in $La_ySr_{1-y}MnO_3$ are Mn^{3+}/Mn^{4+} ions in the ratio $y/(1-y)$. The d shell electronic configuration of Ru^{5+} ions in $SrMn_{1-x}Ru_xO_3$ is identical with that of Mn^{4+} (d^3, t_{2g}^3). Therefore, the ratio of d^4/d^3 ions in both classes of materials is identical, which leads to a very similar structural and magnetic behavior. The paramagnetic Curie-Weiss temperature Θ, also presented in Fig. 7(a), was calculated from the molar dc susceptibility $\chi_m = M/H$ in the temperature range of 350–400 K, which was fitted to the general Curie-Weiss formula,

$$\chi_m = \chi_0 + (\mu_B N_A/3k_B)\mu_{\text{eff}}^2/(T-\Theta), \tag{1}$$

where χ_0 is a temperature-independent background susceptibility, N_A is the Avogadro number, k_B is the Boltzmann constant, Θ is the paramagnetic Curie-Weiss temperature, $\mu_{\text{eff}} = g\sqrt{S(S+1)}$ is the effective paramagnetic moment, $g=2$ is the gyromagnetic ratio, and S is the magnetic spin. The values of Θ pretty well coincide with the values of T_C or T_f.

The effective paramagnetic moment μ_{eff} determined from the magnetization using Eq. (1) is presented in Fig. 7(b). We consider two possible valence states of the Ru dopant, 4+ and 5+. The former case would lead to the formula $SrMn_{1-x}^{4+}Ru_x^{4+}O_3$, and the expected dependence $\mu_{\text{eff}} = \sqrt{\mu_{\text{eff}}^2(\text{Mn}) + \mu_{\text{eff}}^2(\text{Ru})}$, plotted as the dashed line in Fig. 7(b), is far from the observed μ_{eff} behavior. The latter case would give the formulas $SrMn_{1-2x}^{4+}Mn_x^{3+}Ru_x^{5+}O_3$ and $SrMn_{1-x}^{3+}Ru_{1-x}^{5+}Ru_{2x-1}^{4+}O_3$ for $x \leq 0.5$ and $x \geq 0.5$, respectively. These formulas are plotted as solid lines. In both cases we assume spin only moments. The latter model works well for $x \geq 0.5$. This is an additional evidence for the presence of Ru^{5+} ions in this material. However, significant deviations from any of the discussed models can be observed for $x < 0.5$, especially for pure $SrMnO_3$. The determined μ_{eff} values are much lower in this region (not shown). Θ is also positive in the $x < 0.5$ solid solution range, which in turn is a sign of ferromagnetic interactions in the paramagnetic state, even if these compositions exhibit an AF order at low temperatures. It is possible that in this doping regime the fitting temperature range is very close to the magnetic and structural transition temperatures and the Curie-Weiss approximation in Eq. (1) is not fully valid. Another explanation for the reduced μ_{eff} of $SrMnO_3$ and lightly substituted compositions may relate to unusual bond distances observed for these compounds that would require further study.

C. Resistivity

The temperature dependence of resistivity $\rho(T)$ for $SrMn_{1-x}Ru_xO_3$ samples is presented in Fig. 8. The resistivity demonstrates an insulating character for $SrMnO_3$ and overly decreases with increasing Ru substitution due to itinerant character of the Ru electrons. It becomes metallic for $x \geq 0.9$ with a metal to insulator transition at around 70 K for $x=0.9$. The difference between the characters of resistivity for highly Ru-substituted polycrystalline samples and single

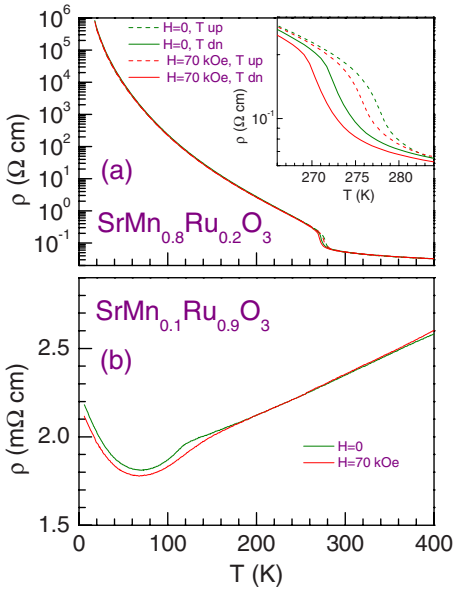

FIG. 9. (Color online) Magnetoresistance for selected $SrMn_{1-x}Ru_xO_3$ samples.

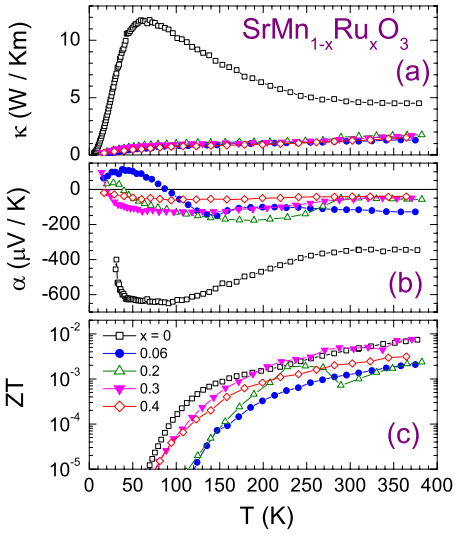

FIG. 10. (Color online) (a) Thermal conductivity, (b) Seebeck coefficient, (c) thermoelectric figure of merit $ZT=\alpha^2T/(\kappa\rho)$ for selected $SrMn_{1-x}Ru_xO_3$ samples.

crystals can be explained by the granular nature of the polycrystalline samples. It has been demonstrated, e.g., for polycrystalline colossal magnetoresistance manganites, that the presence of grain boundaries can affect the magnitude of resistivity as well as the low-temperature magnetoresistance without affecting their magnetic properties. For low Ru contents ($x \leq 0.2$) a significant increase in resistivity is observed below the coupled AF-structural transitions. These transitions correspond to a jump in $\rho(T)$ again similar to rare-earth substituted $SrMnO_3$.[27] This behavior corresponds to a first-order phase transition with a hysteretic behavior of ρ as illustrated in Fig. 9(a). The transition can be shifted to lower temperatures by applying a magnetic field. A slight magnetoresistance can be observed for higher Ru contents below the Curie temperature. Generally, this effect is rather small, although it is enhanced with respect to pure $SrRuO_3$.[9] For $x=0.3$, where the structural and magnetic transitions are decoupled, a subtle anomaly in resistivity can be observed at a temperature related to the structural transition along with a smooth resistivity behavior at the AF transition.

D. Thermoelectric properties

For higher Ru contents it has been demonstrated[24] that the Seebeck coefficient is positive and varies slightly from +34 μV/K for $SrRuO_3$ to +28 μV/K for $SrMn_{0.1}Ru_{0.9}O_3$ at room temperature. This small change reflects the introduction of Ru^{5+} ions into the Ru^{4+} matrix. In Fig. 10, we present thermal conductivity κ, Seebeck coefficient α, and the thermoelectric figure of merit $ZT=\alpha^2T/(\kappa\rho)$ for selected $SrMn_{1-x}Ru_xO_3$ samples. For $SrMnO_3$, α is large and negative (−350 μV/K at RT). A low Ru substitution induces a drastic change in α to values of −50 to −60 μV/K at RT. This negative effect on the thermoelectric properties is compensated by a significant decrease in ρ and κ, which, e.g., gives similar values of ZT at and above room temperature for $x=0.3$ as for pure $SrMnO_3$. We observe a crossover of α from negative to positive values at low temperatures for a low Ru substitution. This crossover shifts to lower temperatures with the Ru substitution. A similar effect has been seen in $SrMnO_3$ with a different B-site substitution (Mo) as well as with an A-site substitution (Pr).[29]

IV. SUMMARY

In summary, we have studied the phase diagram of polycrystalline perovskite $SrMn_{1-x}Ru_xO_3$ ($0 \leq x \leq 1$) system. In the low Ru^{5+} substitution regime ($x \leq 0.3$), the structural, magnetic, and transport behaviors strikingly resemble those for the $SrMnO_3$ compound with an A-site heterovalent substitution $R_ySr_{1-y}MnO_3$ (R=La, Pr). In both cases, a tetragonal lattice distortion, for some compositions, coupled to a C-type AF transition is observed. This similarity is driven by the same ratio of d^4/d^3 ions in both classes of materials for equivalent substitution level. In the moderate Ru^{5+} substitution regime ($x \sim 0.65$) a boundary between the AF-C and FM orders in polycrystalline $SrMn_{1-x}Ru_xO_3$ is broadened with respect to a sharp quantum critical point previously observed in single crystals due to magnetic disorder, which leads to a spin-glass behavior. The observation of a spin-glass behavior suggests that the AF-C and FM states are separated by a first-order transition in the clean limit and they can coexist in the presence of quenched disorder.[30]

ACKNOWLEDGMENTS

Work at NIU was supported by the NSF (Contract No. DMR-0706610). Work at Argonne National Laboratory was supported by the U.S. Department of Energy under Contract No. DE-AC02-06CH11357.

[1] Y. Ying, J. Fan, L. Pi, Z. Qu, W. Wang, B. Hong, S. Tan, and Y. Zhang, Phys. Rev. B **74**, 144433 (2006).
[2] P. V. Vanitha, A. Arulraj, A. R. Raju, and C. N. R. Rao, C.R. Acad. Sci., Ser. IIc: Chim **2**, 595 (1999).
[3] A. Maignan, C. Martin, M. Hervieu, and B. Raveau, Solid State Commun. **117**, 377 (2001).
[4] R. Mathieu, A. Asamitsu, Y. Kaneko, J. P. He, X. Z. Yu, R. Kumai, Y. Onose, N. Takeshita, T. Arima, H. Takagi, and Y. Tokura, Phys. Rev. B **72**, 092404 (2005).
[5] G. Cao, S. Chikara, X. N. Lin, E. Elhami, V. Durairaj, and P. Schlottmann, Phys. Rev. B **71**, 035104 (2005).
[6] R. K. Sahu and S. S. Manoharan, J. Appl. Phys. **92**, 4831 (2002).
[7] R. K. Sahu, Z. Hu, M. L. Rao, S. S. Manoharan, T. Schmidt, B. Richter, M. Knupfer, M. Golden, J. Fink, and C. M. Schneider, Phys. Rev. B **66**, 144415 (2002).
[8] X.-Y. Zhang, Y. Chen, Z.-Y. Li, C. Vittoria, and V. G. Harris, J. Phys.: Condens. Matter **19**, 266211 (2007).
[9] G. N. Banerjee, R. N. Bhowmik, and R. Ranganathan, J. Phys.: Condens. Matter **13**, 9481 (2001).
[10] L. Pi, A. Maignan, R. Retoux, and B. Raveau, J. Phys.: Condens. Matter **14**, 7391 (2002).
[11] B. Dabrowski, S. Kolesnik, O. Chmaissem, T. Maxwell, M. Avdeev, P. W. Barnes, and J. D. Jorgensen, Phys. Rev. B **72**, 054428 (2005).
[12] A. J. Williams, A. Gillies, J. P. Attfield, G. Heymann, H. Huppertz, M. J. Martinez-Lope, and J. A. Alonso, Phys. Rev. B **73**, 104409 (2006).
[13] O. Chmaissem, B. Dabrowski, S. Kolesnik, J. Mais, D. E. Brown, R. Kruk, P. Prior, B. Pyles, and J. D. Jorgensen, Phys. Rev. B **64**, 134412 (2001).
[14] B. Dabrowski, O. Chmaissem, J. Mais, S. Kolesnik, J. D. Jorgensen, and S. Short, J. Solid State Chem. **170**, 154 (2003).
[15] A. Maignan, C. Martin, M. Hervieu, and B. Raveau, J. Appl. Phys. **91**, 4267 (2002).
[16] Z. H. Han, J. I. Budnick, W. A. Hines, B. Dabrowski, and T. Maxwell, Appl. Phys. Lett. **89**, 102501 (2006).
[17] D. G. Hinks, B. Dabrowski, J. D. Jorgensen, A. W. Mitchell, D. R. Richards, and D.-L. Shi, Nature (London) **333**, 836 (1988).
[18] J. D. Jorgensen, J. J. Faber, J. M. Carpenter, R. K. Crawford, J. R. Haumann, R. L. Hitterman, R. Kleb, G. E. Ostrowski, F. J. Rotella, and T. G. Worton, J. Appl. Crystallogr. **22**, 321 (1989).
[19] A. C. Larson and R. B. von Dreele, General Structure Analysis System (GSAS), Los Alamos National Laboratory Report No. LAUR 86-748, 2004 (unpublished); B. H. Toby, J. Appl. Crystallogr. **34**, 210 (2001).
[20] T. Taniguchi, S. Mizusaki, N. Okada, Y. Nagata, S. H. Lai, M. D. Lan, N. Hiraoka, M. Itou, Y. Sakurai, T. C. Ozawa, Y. Noro, and H. Samata, Phys. Rev. B **77**, 014406 (2008).
[21] I. D. Brown and D. Altermatt, Acta Crystallogr., Sect. B: Struct. Sci. **41**, 244 (1985).
[22] B. J. Kennedy and B. A. Hunter, Phys. Rev. B **58**, 653 (1998).
[23] B. Dabrowski, M. Avdeev, O. Chmaissem, S. Kolesnik, P. W. Klamut, M. Maxwell, and J. D. Jorgensen, Phys. Rev. B **71**, 104411 (2005).
[24] Y. Klein, S. Hébert, A. Maignan, S. Kolesnik, T. Maxwell, and B. Dabrowski, Phys. Rev. B **73**, 052412 (2006).
[25] J. Pietosa, A. Wisniewski, R. Puzniak, S. Kolesnik, M. Majjiga, and B. Dabrowski, Acta Phys. Pol. A **111**, 159 (2007).
[26] B. Dabrowski, O. Chmaissem, P. W. Klamut, S. Kolesnik, M. Maxwell, J. Mais, Y. Ito, B. D. Armstrong, J. D. Jorgensen, and S. Short, Phys. Rev. B **70**, 014423 (2004).
[27] O. Chmaissem, B. Dabrowski, S. Kolesnik, J. Mais, J. D. Jorgensen, and S. Short, Phys. Rev. B **67**, 094431 (2003).
[28] S. Kolesnik, B. Dabrowski, J. Mais, D. E. Brown, R. Feng, O. Chmaissem, R. Kruk, and C. W. Kimball, Phys. Rev. B **67**, 144402 (2003).
[29] A. Maignan, S. Hébert, L. Pi, D. Pelloquin, C. Martin, C. Michel, M. Hervieu, and B. Raveau, Cryst. Eng. **5**, 365 (2002).
[30] J. Burgy, M. Mayr, V. Martin-Mayor, A. Moreo, and E. Dagotto, Phys. Rev. Lett. **87**, 277202 (2001).